Preprints of the 21st IFAC World Congress (Virtual)
Berlin, Germany, July 12-17, 2020

Path Planning and Tracking for Autonomous Vehicle Collision Avoidance with Consideration of Tire-Road Friction Coefficient ⋆

Juqi Hu, Youmin Zhang and Subhash Rakheja

Department of Mechanical, Industrial and Aerospace Engineering, Concordia University, Montreal, Canada, (e-mails: hujuqi89@gmail.com; youmin.zhang@concordia.ca; subhash.rakheja@concordia.ca).

Abstract: Autonomous vehicles (AVs) have attracted a lot of attention in recent years and fully-autonomous vehicles are expected on road in the near future. Collision avoidance is one of the key driving tasks for autonomous driving which consists of path planning and tracking control. The main problem discussed in this paper is the development of a path planning and tracking framework based on model predictive control (MPC) with consideration of the estimated tire-road friction coefficient (TRFC). The planned path in terms of lateral position is generated based on the safety distance between the host and the obstacle vehicle, which is related to TRFC and vehicle speed. A new structure of MPC is further designed so that only lateral position is required to track the planned path. Moreover, the adaptive weights on the outputs to a wide range of vehicle speeds have been identified. The effectiveness of the proposed planning and tracking framework is validated through CarSim-MATLAB/Simulink co-simulations on both high- and low-friction roads.

Keywords: Autonomous vehicles, Path planning, Path tracking, Model-based control, Tire-road friction coefficient.

1. INTRODUCTION

Autonomous vehicles (AVs) have great potential to achieve improved driving safety, passenger's comfort and traffic efficiency and thus attracted considerable interests and efforts from academia, industry and governments, see Li et al. (2017); Anderson et al. (2014) and Gill et al. (2015). The significant advances in sensing, computing and artificial technologies, particularly in the last decade, have further inspired the whole society's expectation and passion for commercially-viable AVs (Cohen and Hopkins, 2019). Path planning and tracking control play a critical role in autonomous driving, which refer to the determination of the AVs' collision-free path from the vehicle's current location to a designated target in accordance with the traffic rules, safety, comfortability and vehicular dynamics. There is substantial research on path planning and tracking control for AVs and very good reviews on various planning algorithms and control methods can be found in Katrakazas et al. (2015); You et al. (2015). In order to find the best path to follow, different types of constraints imposed by vehicle dynamics, actuator saturation, road boundary, should be taken into consideration while meeting the requirement of obstacle avoidance. Due to its capability of handling constraints in a systematic way, model predictive control (MPC) technique has recently become an appealing method to solve the AVs' path planning and tracking control problems (Li et al., 2017; Gao et al., 2011). The approach involves optimizing a performance index under operation constraints with respect to a sequence of control inputs to generate a desired path or to track a given trajectory by applying the first element of such optimal input sequence to the vehicle system (Gao et al., 2011; Dixit et al., 2018). Two different research directions can be seen in the reported studies. Some researchers integrated the control module with the path planner respecting the fact that path planning and tracking control have strong connection to each other. Jalalmaab et al. (2016) investigated a road-adaptive MPC strategy to track the centerline of the lane while avoiding the obstacle. Although path planning and tracking were realized within one linear MPC framework, it should be noted that only kinematic point-mass vehicle model was used to ensure real-time implementation. In order to take into account both the tire force saturation and the vehicle nonlinearities, a nonlinear MPC based on a four-wheel vehicle model and a Magic Formula tire model was designed to conduct path re-planning and tracking task in Gao et al. (2011). The experimental results have shown that the computation time increases rapidly and induced an issue of real-time implementation when the vehicle speed is over 40 km/h.

To avoid complex optimization process which may result in excessive computational demand, an alternative way is to address the path planning and tracking problem separately in a hierarchical architecture. In the project of PRORETA

⋆ This work was partially supported by the Natural Sciences and Engineering Research Council of Canada (NSERC) and the Concordia University Seed Funding Program.

3, Bauer et al. (2012) utilized a potential field-based trajectory planner to calculate the optimal vehicle trajectory, which is then fed into the control layer to achieve collision avoidance in critical traffic situations. In Ji et al. (2016), the collision-free path for AVs was generated based on a three-dimensional potential field method considering road boundary conditions and vehicle's kinematic model. The commanded steering angle to track the generated path was then obtained from a multi-constrained MPC framework. Similarly, Shim et al. (2012) designed a collision avoidance system which determined a collision-free trajectory based on sixth-order polynomials, and the front steering and individual wheel torques were controlled by an MPC scheme to track the reference path. When the nonlinear vehicle model was used in the MPC, the linearization technique can be applied in each prediction step to reduce the computational burden, as shown in Yi et al. (2016). In addition to computational burden, the structure of the cost function and the tuning weights on outputs and inputs also have heavy impact on the performance of MPC. Unfortunately, relatively less efforts have been made toward this field. Another issue is related to the tire-road friction coefficient (TRFC), which reflects the limitation of the available force the road can provide to a vehicle. This coefficient is closely linked to direction control and stability performance of a road vehicle and is especially important for AVs since they should be able to perform driving tasks on different road conditions. Most of the previous works in a hierarchical architecture only introduce the TRFC to the path tracking module as input and/or state constraints, such as Yi et al. (2016); Gao et al. (2011) and Ji et al. (2016). Actually, the quality or smoothness of the reference path has a significant influence on the tracking control performance. Thus, considering the limitation of the road friction earlier in the high-level path planner can significantly simplify the design of the low-level tracking controller.

In this paper, we focus on the two-level path planning and tracking for an autonomous vehicle to avoid vehicle collision on a straight one-way, two-lane highway. It is assumed that road boundaries, lane centerlines and forward speeds of both the host and the obstacle vehicles are all available from the on-board sensors (e.g., LiDAR, Radar), and a double-lane change (DLC) maneuver on roads with different friction levels is considered. In the high-level planning module, a TRFC-based path for DLC is generated by making use of the road friction and vehicle speed information. With the front tire steer angle as the control input, a linear dynamic MPC with adaptive weights on outputs in the cost function is further designed to follow the planned path as close as possible under a wide range of forward speeds. The proposed planning and tracking framework will be described in detail in the following sections.

2. PATH PLANNING FOR LANE CHANGING

The scenario of a DLC vehicle collision avoidance is shown in Fig. 1. XOY is the absolute inertial frame with X-axis defined positive to the right along the centerline of lane 1, Y-axis defined positive upward along the perpendicular of the lane centerline. To simplify the generation of the collision-free path, this paper only focuses on the following conditions: (i) The host vehicle A is drived at a constant

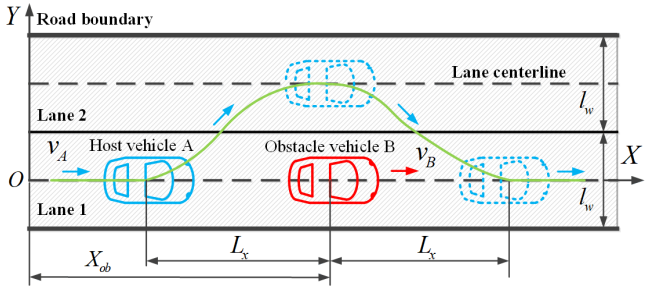

Fig. 1. A DLC scenario of vehicle collision avoidance

forward speed v_A all the time and moving along the centerline of lane 1 before the lane changing maneuver; (ii) The obstacle vehicle B is static or moving at a very low speed $v_B \leqslant \frac{v_A}{3}$ ahead of vehicle A along the centerline of lane 1; (iii) There is no vehicle in lane 2 which is available for lane changing.

As the host vehicle A is approaching to the obstacle vehicle B, lane change maneuver has to be conducted when a collision cannot be avoided through braking alone. A conservative safety distance, which is used to determine when the lane changing maneuver is necessary relevant to both the TRFC (μ) and the vehicle speeds (v_A, v_B), is defined as:

$$L_x = (v_A^2 - v_B^2)/2\mu g + v_A * h_0 + d_0 + l \tag{1}$$

where the first term represents the minimum braking distance required to reduce speed from v_A to v_B, with $g = 9.81$ m/s^2 being the acceleration due to gravity; h_0 and d_0 are headway time and standstill distance, respectively; l is the wheelbase which is added here for consideration of vehicle geometry. Based on the continuous-curvature path proposed by Nelson (1989), the safety distance is utilized to generate the desired path of the host vehicle A, which is defined by representing lateral position Y_d as a function of the longitudinal position X, and is expressed as:

$$Y_d = \begin{cases} l_w[10(\frac{X_3}{L_x})^3 - 15(\frac{X_3}{L_x})^4 + 6(\frac{X_3}{L_x})^5], \ X_1 \leqslant X \leqslant X_{ob} \\ l_w[10(\frac{X_4}{L_x})^3 - 15(\frac{X_4}{L_x})^4 + 6(\frac{X_4}{L_x})^5], \ X_{ob} < X \leqslant X_2 \\ 0, \text{ else} \end{cases} \tag{2}$$

where l_w is the lane width, $X_1 = X_{ob} - L_x$, $X_2 = X_{ob} + L_x$, $X_3 = X - X_1$, $X_4 = 2X_{ob} - X_1 - X$, with X_{ob} being the longitudinal position of the vehicle B as shown in Fig. 1. By following the reference path (2), vehicle A starts steering from the centerline of lane 1 to the adjacent lane 2 at $X = X_1$, reaches the centerline of lane 2 at $X = X_{ob}$, and goes back to the original centerline at $X = X_2$. The smoothness of the desired path and the duration of the DLC maneuver are determined by the safety distance L_x, and thus related to the TRFC and vehicle speeds. This is a simple way which may mimic a skillful driver taking the road friction condition and vehicle speed into account on highway.

Remark 1. It is evident from (1) and (2) that the lower v_A the sharper path will be generated. It may become difficult to follow the desired path when the host vehicle is running at a very low speed. $v_A \geqslant 30$ km/h is thus considered in this paper and this is reasonable especially for studying DLC maneuver on highway.

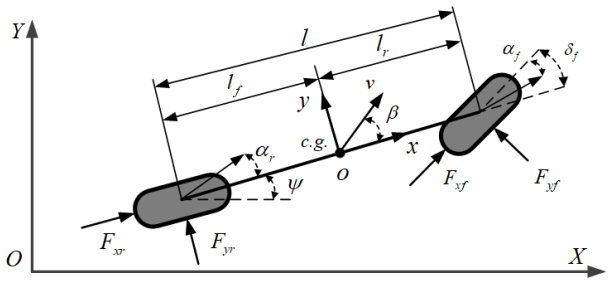

Fig. 2. Simplified one-track model used for path tracking

Remark 2. The friction coefficient (μ) is assumed having been estimated before the DLC maneuver when the vehicle is driving on the straight road. More details about the TRFC estimation can be referred to authors' previous work (Hu et al., 2019).

3. PATH TRACKING CONTROLLER DESIGN

3.1 Vehicle Dynamic Model

Considering constant longitudinal velocity, a simplified one-track model of a vehicle is selected to describe the lateral motion, as shown in Fig. 2. The vehicle body frame xoy is centered on the center of gravity ($c.g.$), with x defined positive to the right along the centerline of the vehicle and y defined positive upward along the perpendicular of x. The motion equations of this model can be derived with the help of force and torque balances with respect to the $c.g.$ and coordinate transformations between the inertial frame and the vehicle body frame:

$$\begin{aligned} m(\dot{v}_y + v_x\dot{\psi}) &= F_{yf} + F_{yr} \\ I_z\ddot{\psi} &= l_f F_{yf} - l_r F_{yr} \\ \dot{Y} &= v_x\psi + v_y \end{aligned} \tag{3}$$

where m is the vehicle mass, I_z is the rotational inertia about the z-axis, l_f and l_r are the distances from the $c.g.$ to the front- and rear-axle, respectively. v_x, v_y are the vehicle longitudinal and lateral velocities in the body frame. $\psi, \dot{\psi}$ and Y are yaw angle, yaw rate and lateral position of the host vehicle in the inertial frame, respectively. For small tire slip angle, the unknown cornering force of front- and rear-axle, F_{yf} and F_{yr}, are approximated as a linear function of tire slip angle as:

$$F_{yi} = -2C_i \cdot \alpha_i,\ i = f, r \tag{4}$$

where C_i and α_i are the individual tire cornering stiffness and the tire slip angle, $i = f, r$ represents front and rear tires, respectively. Using small angle approximation, the tire slip angle (α_f, α_r) are described by Ahn et al. (2013):

$$\begin{aligned} \alpha_f &= (v_y + l_f\dot{\psi})/v_x - \delta_f \\ \alpha_r &= (v_y - l_r\dot{\psi})/v_x \end{aligned} \tag{5}$$

where δ_f is the front tire steer angle.

3.2 MPC Controller Formulation

The state-space vehicle model for the MPC optimization process is derived based on the equations (3)-(5), and this model can be compactly written as:

$$\begin{aligned} \dot{x}(t) &= Ax(t) + Bu(t) \\ z(t) &= Cx(t) \end{aligned} \tag{6}$$

where $x(t) \in \mathbb{R}^n$ is the state of the system, $u(t) \in \mathbb{R}^m$ is the input and $z(t) \in \mathbb{R}^p$ is the output, $n = 4$ is the number of states, $m = 1$ is the number of input and $p = 3$ is the number of outputs. The four states are lateral velocity in the body frame, yaw angle, yaw rate, and lateral coordinates of the $c.g.$ of the host vehicle in the inertial frame. These are denoted respectively as $x = [v_y, \psi, \dot{\psi}, Y]'$. The only input for lateral control is the front tire steering angle $u = \delta_f$. The three outputs are denoted as $z = [\dot{\psi}, Y, \beta]'$ where β is the vehicle's sideslip angle. The matrices A, B and C in (6) are listed as:

$$A = \begin{bmatrix} -\dfrac{2C_f + 2C_r}{mv_x} & 0 & -v_x - \dfrac{2C_f l_f - 2C_r l_r}{mv_x} & 0 \\ 0 & 0 & 1 & 0 \\ -\dfrac{2l_f C_f - 2l_r C_r}{I_z v_x} & 0 & -\dfrac{2l_f^2 C_f + 2l_r^2 C_r}{I_z v_x} & 0 \\ 1 & v_x & 0 & 0 \end{bmatrix} \tag{7}$$

$$B = \begin{bmatrix} \dfrac{2C_f}{m} \\ 0 \\ \dfrac{2l_f C_f}{I_z} \\ 0 \end{bmatrix},\ C = \begin{bmatrix} 0 & 0 & 1 & 0 \\ 0 & 0 & 0 & 1 \\ \dfrac{1}{v_x} & 0 & 0 & 0 \end{bmatrix}$$

In order to obtain a finite-dimensional optimal control problem, we discretize the system dynamics (6) with a fixed sampling time T_s using Euler's method:

$$\begin{aligned} x(k+1|k) &= A_d \cdot x(k|k) + B_d \cdot u(k|k) \\ z(k|k) &= C_d \cdot x(k|k) \end{aligned} \tag{8}$$

where $A_d = E + AT_s, B_d = BT_s$ and $C_d = C$, with E an n-dimensional unit matrix.

Let k be the current time step, $x_k = x(k|k)$ is the state vector at k-th step and consider the following cost function:

$$\begin{aligned} J(x_k, \mathcal{U}_k, \epsilon_k) = &\sum_{i=1}^{H_p} \|\eta(k+i|k) - \eta^r(k+i|k)\|_Q^2 \\ &+ \sum_{i=0}^{H_c-1} \|\Delta u(k+i|k)\|_R^2 + \rho\epsilon_k^2 \end{aligned} \tag{9}$$

where $\eta(k+i|k) = z(k+i|k)$ represent the predictive outputs and $\eta^r(k+i|k)$ are the corresponding reference signals at sampling step $k+i$. $\Delta u(k+i|k) = u(k+i|k) - u(k+i-1|k)$ are the differences of the control inputs at sampling step $k+i$ and $u(k-1|k)$ are the known inputs from the previous control interval. $\mathcal{U}_k = [u(k|k)', ..., u(k+H_c-1)']'$ is the optimization vector at time step k. H_p and H_c are the prediction and control horizon respectively, and $H_p > H_c$. To reduce computational requirement, the control signal sequences $u(k+i|k)$ hold equal to $u(k+H_c-1|k)$ while $H_c \leqslant i \leqslant H_p$. The term $\rho\epsilon_k^2$ penalizes the violation of the constraint, ϵ_k is a slack variable and ρ is a weighting coefficient. Q and R are diagonal matrices with the squares of those output weights and input rate weights, respectively, being the diagonal elements. They are written as $Q = \mathrm{diag}(\lambda_1^2, \lambda_2^2, \lambda_3^2)$, $R = \lambda_4^2$.

The objective of the MPC controller is to track the desired path generated in Section 2. As shown in (2), only reference lateral position is directly generated. However, the host vehicle is driving on a straight line before and after

the lane change maneuver. Considering the physical characteristics, the reference values of both the yaw rate and vehicle sideslip angle can be set zero before and after the DLC maneuver. Still, the reference vehicle sideslip angle and yaw rate during the DLC maneuver are unknown. In this case, the above optimal problem (9) can not be solved through a traditional MPC scheme. Here, we propose a new way to deal with this problem and the prerequisite is only the reference lateral position.

Remind that the higher the output weights, the higher demand on tracking the corresponding reference signal. The controller will ignore the setpoints with zero weight and allow the output to vary freely. Based on this, the weight on the predictive output is set to zero when there is lack of its reference value. Thus, the output weight on yaw rate (λ_1) is set zero during the DLC maneuver and a nonzero value otherwise. Unlike yaw rate being an easily measured signal, vehicle sideslip angle is hard to be directly measured, its output weight is thus setting to zero all the time ($\lambda_3 = 0$). Doing so will enable the vehicle sideslip angle and yaw rate to vary freely around their respective setpoints when no reference values are given. The setpoints of vehicle sideslip angle and yaw rate are assigned both zero in $\eta^r(k+i|k)$ for respecting the fact that the host vehicle is starting from the centerline and going back to the same centerline. Moreover, it is not safe when the generated yaw rate or vehicle sideslip angle is beyond the value the road is able to provide (Rajamani, 2011). At high vehicle sideslip angle, the tires may lose their linear behavior and cause large tracking errors. Hence the magnitude of these two outputs should be bounded by the friction-related constraints. At each time step k, the following finite horizon optimal control problem is solved:

$$
\begin{aligned}
&\min_{\mathcal{U}_k,\epsilon_k} J(x_k,\mathcal{U}_k,\epsilon_k)\\
\text{s.t. }\ & x(k+1|k) = A_d\cdot x(k|k) + B_d\cdot u(k|k)\\
& \eta(k|k) = C_d\cdot x(k|k)\\
& u(k-1|k) = u(k-1)\\
& \Delta u(k+i|k) = u(k+i|k) - u(k+i-1|k)\\
& \Delta u_{min} \leqslant \Delta u(k+i|k) \leqslant \Delta u_{max}\\
& u_{min} \leqslant u(k+i|k) \leqslant u_{max}\\
& i = 0,...,H_c-1\\
& \Delta u(k+i|k) = 0,\ i = H_c,...,H_p\\
& \begin{bmatrix}\dot\psi_{min}\\ Y_{min}\\ \beta_{min}\end{bmatrix} - \epsilon_k \leqslant \eta(k+i|k) \leqslant \begin{bmatrix}\dot\psi_{max}\\ Y_{max}\\ \beta_{max}\end{bmatrix} + \epsilon_k\\
& i = 1,...,H_p,\ \epsilon_k \geqslant 0\\
& x(k|k) = x_k,\ \eta^r(k+i|k) = [0\ \ Y_d\ \ 0]'
\end{aligned}
\tag{10}
$$

where u_{min} and Δu_{min}, u_{max} and Δu_{max} are the constraints imposed on the control signals. The constraints exerted on the output variables are denoted in Table 1 with l_w and t_w being lane width and wheel track width, respectively. The empirical selection of the friction-related upper and lower bounds of $\dot\psi$ and β can be referred to Rajamani (2011).

Remark 3. Vehicle sideslip angle β is approximated as v_y/v_x and the output constraint $\beta_{min}-\epsilon_k \leqslant \beta \leqslant \beta_{max}+\epsilon_k$ is transferred to state constraint on vehicle lateral velocity.

The optimization problem (10) can be recast as a quadratic program and it does not require any complex optimization software. Denoted by $\mathcal{U}_k^* = [u^*(k|k)', ..., u^*(k+H_c-1)']'$, the sequence of optimal inputs are computed at time step k by solving (10) for the current system states x_k, then the first sample of $\mathcal{U}_k^*$ is applied to the vehicle at time k. At time $k+1$, a new optimization is solved over a shifted prediction horizon starting from the newly measured states $x(k+1|k+1) = x_{k+1}$.

Table 1. Constraints on outputs

Outputs	Minimum value	Maximum value
$\dot\psi$	$-0.85\mu g/v_x$	$0.85\mu g/v_x$
Y	$-l_w/2 + t_w/2$	$3l_w/2 - t_w/2$
β	$-\arctan(0.02\mu g)$	$\arctan(0.02\mu g)$

3.3 Adaptive Weights in Cost Function

The performance of the above MPC is strongly related to the tuning weight set $\lambda = [\lambda_1, \lambda_2, \lambda_3, \lambda_4]$. Given a vehicle forward speed, it is easy to tune a set of λ to achieve acceptable tracking results. However, the performance of the controller with fixed values of λ will be degraded or even unacceptable (cause oscillations and instability) when the vehicle is moving under a different velocity. A straightforward method is to design the adaptive weights varying with vehicle speed. While there are four weights to be tuned, the output weights on yaw rate and lateral position (λ_1, λ_2) have larger influence on the performance of the controller than the input weight. Noted that the output weight on vehicle sideslip angle λ_3 is zero as explained in Section 3.2, only λ_1 and λ_2 are needed to set as speed-adaptive values by setting $\lambda_4 = 0.5$. In order to further simplify the tuning process, we set output weight on lateral position as fixed value of $\lambda_2 = 1$. Based on the principle that the higher forward speed, the higher weights should be imposed on yaw rate to ensure vehicle's stability. The adaptive weights on yaw rate were selected after extensive simulations under a wide range of speeds, as shown in Table 2.

Table 2. Adaptive weights

v_x (km/h)	λ_1	v_x (km/h)	λ_1
(30, 50]	0.4	(70, 80]	4.0
(50, 60]	1.0	(80, 92]	6.0
(60, 70]	2.8		

4. SIMULATION RESULTS

To test the performance of the proposed planning and tracking framework, a series of collision avoidance maneuvers at different forward speeds have been conducted using CarSim and MATLAB/Simulink software. Two different road surfaces with friction coefficients of 0.8 and 0.3, denoted as high-μ and low-μ road, respectively, have been set in CarSim. The main parameters for the vehicle model and the highway road used in simulation are shown as:

- $m = 1,416$ kg, $I_z = 1,523$ kgm^2, $l_f = 1.016$ m, $l_r = 1.562$ m, $l = 2.578$ m, $t_w = 1.739$ m, $C_f = 47,000$ N/rad, $C_r = 38,000$ N/rad
- $l_w = 3.5$ m, $h_0 = 2$ s, $d_0 = 2$ m

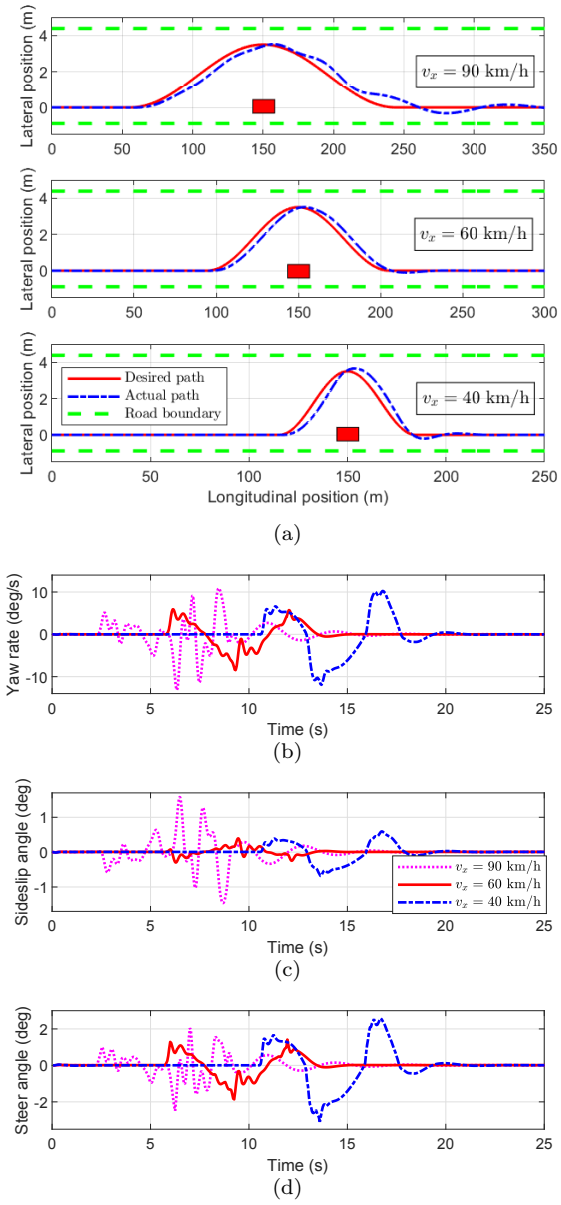

Fig. 3. Simulation results on $\mu = 0.8$ road under three different forward speeds. (a) Desired and actual path (the red box represents the obstacle vehicle). (b) Yaw rate. (c) Vehicle sideslip angle. (d) Steering angle

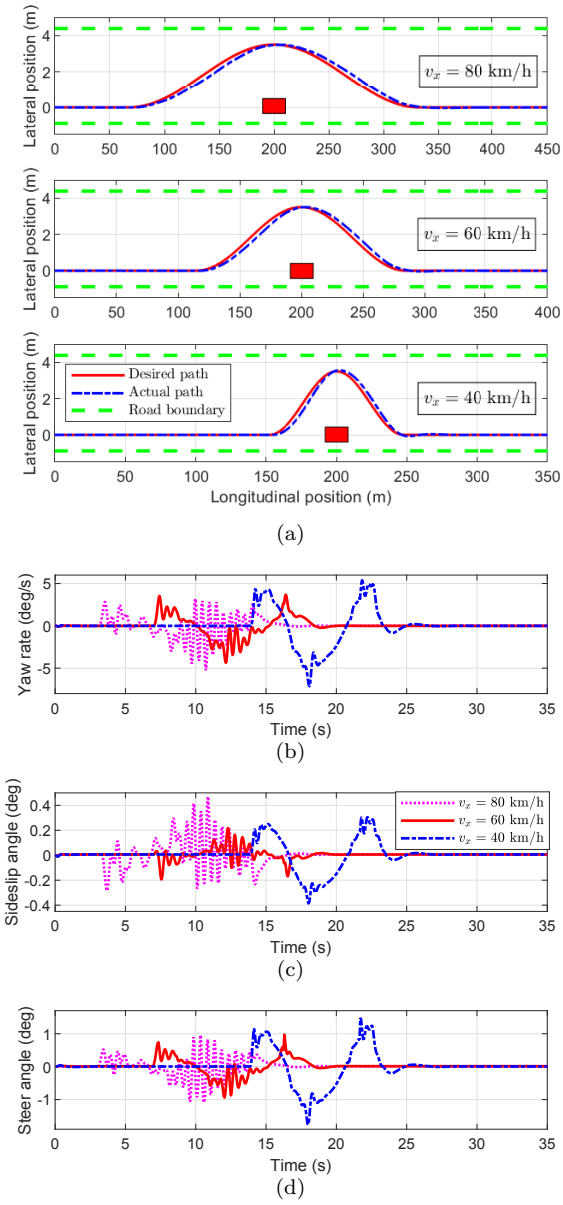

Fig. 4. Simulation results on $\mu = 0.3$ road under three different forward speeds. (a) Desired and actual path (the red box represents the obstacle vehicle). (b) Yaw rate. (c) Vehicle sideslip angle. (d) Steering angle

The adaptive MPC (10) is with the following parameters:

- $T_s = 0.05$ s, $H_p = 15$, $H_c = 5$
- $u \in [-10°, 10°]$, $\Delta u \in [-1°, 1°]$
- $Q = \text{diag}(\lambda_1^2, 1, 0)$, $R = 0.5^2$, $\rho = 10^5$

4.1 High-μ Road

A relatively high friction coefficient ($\mu = 0.8$) was firstly selected to simulate the usual running condition on concrete or asphalt surfaces for highway vehicles. The host and obstacle vehicle were initially located at longitudinal position 0 and 150 m, respectively. The host vehicle's DLC maneuvers under three constant forward speeds $v_x = 90, 60, 40$ km/h, respectively, have been conducted. The three desired paths, corresponding to the different speeds, are computed based on (2), as shown in Fig. 3(a). The higher the forward speed, the earlier the host vehicle starts steering to the adjacent lane and thus leaving larger safety distance. The designed MPC tracks the desired path well and tightly confines the vehicle's position within the road boundaries, though a slightly larger error is observed under 90 km/h. The generated yaw rate, vehicle sideslip angle and wheel steer angle are shown in Figs. 3(b)-3(d). All of these three variables are varying with peak values much smaller than their respective bounds showing the smoothness of the generated paths. As can be seen from Fig. 3(c), the magnitude of the generated vehicle sideslip angle under 90 km/h is much larger than that under two lower speeds. This shows the vehicle forward speed has a strong influence on the sideslip angle and may generate high sideslip angle leading to unstable system. Higher sideslip angle also results in larger vehicle modeling errors,

which partly explains a slight tracking oscillation under 90 km/h. It is also pointed out that the designed MPC is able to obtain acceptable closed-loop performance up to $v_x = 92$ km/h on high-μ road.

4.2 Low-μ Road

The friction coefficient was set as $\mu = 0.3$ to simulate road conditions covered by snow in winter of highway. The host vehicle was initialized at longitudinal position 0 m. The location of the obstacle vehicle was set as $X_{ob} = 200$ m considering that larger safety distance is required on a slippery road under the same speed. Collision avoidance scenarios under three speeds $v_x = 80, 60, 40$ km/h have been investigated. The desired and the actual paths are shown in Fig. 4(a). Compared to those results obtained on high-μ road, the designed MPC can achieve better tracking performance on this low-μ road. This is because the generated paths based on a larger safety distance on the slippery road are smoother. Figs. 4(b)-4(d) demonstrate the generated yaw rate, vehicle sideslip angle and the road wheel steer angle during the DLC maneuver. Due to a poor road adhesion, the commanded wheel steer angle changes more frequently than that on high-μ road to closely track the desired path. As a result, both the yaw rate and the vehicle sideslip angle also rapidly change with time during the lane-change maneuver. The higher the forward speed, the more rapid changes are observed. Again, it is also pointed out that the upper bound of the forward speed for the MPC to stabilize the vehicle and accurately track the desired path is $v_x = 82$ km/h.

5. CONCLUSIONS

An MPC-based path planning and tracking framework for AVs using the estimated TRFC is presented. The desired path is generated based on the safety distance between the host vehicle and the obstacle vehicle which is related to both the TRFC and the vehicle speed. With integrated consideration of output weights in the cost function and the constraints on the magnitude of the outputs defined by the TRFC, a new model predictive controller is designed so that only lateral position is required to track the desired path. Moreover, adaptive weights on outputs in the cost function have been identified making the designed controller applicable to a wide range of speeds.

REFERENCES

Ahn, C., Peng, H., and Tseng, H.E. (2013). Robust estimation of road frictional coefficient. *IEEE Transactions on Control Systems Technology*, 21(1), 1–13.

Anderson, J.M., Nidhi, K., Stanley, K.D., Sorensen, P., Samaras, C., and Oluwatola, O.A. (2014). *Autonomous Vehicle Technology: A Guide for Policymakers*. Rand Corporation.

Bauer, E., Lotz, F., Pfromm, M., Schreier, M., Abendroth, B., Cieler, S., Eckert, A., Hohm, A., Lüke, S., Rieth, P., et al. (2012). Proreta 3: An integrated approach to collision avoidance and vehicle automation. *at-Automatisierungstechnik Methoden und Anwendungen der Steuerungs-, Regelungs-und Informationstechnik*, 60(12), 755–765.

Cohen, S.A. and Hopkins, D. (2019). Autonomous vehicles and the future of urban tourism. *Annals of Tourism Research*, 74, 33–42.

Dixit, S., Fallah, S., Montanaro, U., Dianati, M., Stevens, A., Mccullough, F., and Mouzakitis, A. (2018). Trajectory planning and tracking for autonomous overtaking: State-of-the-art and future prospects. *Annual Reviews in Control*, 45, 76–86.

Gao, Y., Lin, T., Borrelli, F., Tseng, E., and Hrovat, D. (2011). Predictive control of autonomous ground vehicles with obstacle avoidance on slippery roads. In *ASME 2010 Dynamic Systems and Control Conference*, 265–272.

Gill, V., Kirk, B., Godsmark, P., and Flemming, B. (2015). Automated vehicles: The coming of the next disruptive technology. In *Report, Conference Board of Canada, Ottawa*.

Hu, J., Rakheja, S., and Zhang, Y. (2019). Tire-road friction coefficient estimation under constant vehicle speed control. *IFAC-PapersOnLine*, 52(8), 136–141.

Jalalmaab, M., Pirani, M., Fidan, B., and Jeon, S. (2016). Cooperative road condition estimation for an adaptive model predictive collision avoidance control strategy. In *2016 IEEE Intelligent Vehicles Symposium*, 1072–1077.

Ji, J., Khajepour, A., Melek, W.W., and Huang, Y. (2016). Path planning and tracking for vehicle collision avoidance based on model predictive control with multiconstraints. *IEEE Transactions on Vehicular Technology*, 66(2), 952–964.

Katrakazas, C., Quddus, M., Chen, W.H., and Deka, L. (2015). Real-time motion planning methods for autonomous on-road driving: State-of-the-art and future research directions. *Transportation Research Part C: Emerging Technologies*, 60, 416–442.

Li, X., Sun, Z., Cao, D., Liu, D., and He, H. (2017). Development of a new integrated local trajectory planning and tracking control framework for autonomous ground vehicles. *Mechanical Systems and Signal Processing*, 87, 118–137.

Nelson, W. (1989). Continuous-curvature paths for autonomous vehicles. In *Proceedings of 1989 International Conference on Robotics and Automation*, 1260–1264. IEEE.

Rajamani, R. (2011). *Vehicle Dynamics and Control*. Springer Science & Business Media.

Shim, T., Adireddy, G., and Yuan, H. (2012). Autonomous vehicle collision avoidance system using path planning and model-predictive-control-based active front steering and wheel torque control. *Proceedings of the Institution of Mechanical Engineers, Part D: Journal of Automobile Engineering*, 226(6), 767–778.

Yi, B., Gottschling, S., Ferdinand, J., Simm, N., Bonarens, F., and Stiller, C. (2016). Real time integrated vehicle dynamics control and trajectory planning with MPC for critical maneuvers. In *2016 IEEE Intelligent Vehicles Symposium*, 584–589.

You, F., Zhang, R., Lie, G., Wang, H., Wen, H., and Xu, J. (2015). Trajectory planning and tracking control for autonomous lane change maneuver based on the cooperative vehicle infrastructure system. *Expert Systems with Applications*, 42(14), 5932–5946.